RESEARCH ARTICLE OPEN ACCESS

Structural, Vibrational, and Electronic Properties of ZnS Nanoclusters: A DFT study

Umamageswari [1], R. Padmavathi[2]

[1]*(Department of Physics, Binod Bihari Mahto Koyalanchal University, Dhanbad, Jharkhand-826001, India)*
uma51068@gmail.com
[2]*(Department of Physics, Meenakshi Sundararajan Engineering College, Kodambakkam, Chennai-600024, India.)* **pathmavati@gmail.com**

----------**********----------

Abstract:

Zinc sulphide (ZnS) is a wide band gap II–VI semiconductor with significant applications in optoelectronic devices, sensors, photocatalysis, and ultraviolet photodetectors. In the present study, a comprehensive Density Functional Theory (DFT) investigation was performed to evaluate the structural, vibrational, electronic, and optical properties of ZnS. Geometry optimization and frequency calculations were carried out using the B3LYP hybrid functional in combination with the 6-31G(d,p) basis set for sulphur and LANL2DZ effective core potential for zinc. The optimized Zn–S bond parameters confirm structural stability with no imaginary frequencies. Simulated FTIR and Raman spectra reveal characteristic Zn–S vibrational modes consistent with reported experimental data. Frontier molecular orbital analysis shows a significant HOMO–LUMO energy gap, confirming the semiconducting nature of ZnS. Mulliken population analysis and electrostatic potential (ESP) mapping indicate charge transfer from Zn to S atoms, reflecting partial ionic character. Electron density and contour plots further support bonding interactions. Time-dependent DFT (TD-DFT) calculations were employed to predict UV–Vis absorption behaviour, and the optical band gap was correlated using Kubelka–Munk analysis. The results provide detailed insight into the fundamental electronic and optical behaviour of ZnS, supporting its suitability for advanced optoelectronic applications. DFT and TD-DFT analyses confirm ZnS nanoparticles as stable wide-bandgap semiconductors with promising applications in solar energy conversion and nanophotonic devices.

Keywords **— FTIR, FT-Raman, HOMO-LUMO, Mulliken, MEP, Fukui functions**

----------**********----------

I INTRODUCTION

ZnS is a technologically important II–VI semiconductor, widely investigated due to its wide direct band gap (~3.6–3.8 eV), high transparency in the visible region, and excellent luminescent properties [1]. Commonly used photoconductive films include CdS, ZnS, CdSe, ZnSe, CdTe, GaAs, Ge, Si, PbS, and certain organic materials [2]. ZnS exists mainly in two crystalline phases—zinc blende (cubic) and wurtzite (hexagonal)—both of which exhibit unique optical and electronic characteristics. Owing to these properties, ZnS has been extensively applied in light-emitting diodes, photovoltaic devices, photocatalysis, sensors, electroluminescent devices, and UV photodetectors**.**

Understanding the structural and electronic properties of ZnS at the atomic level is crucial for improving its performance in nanoscale and optoelectronic applications. Experimental techniques such as FTIR, Raman spectroscopy, and UV–Vis spectroscopy provide valuable information about vibrational and optical behaviour; however, theoretical approaches, particularly Density Functional Theory (DFT), offer deeper insight into electronic structure, charge distribution, and bonding characteristics. All DFT calculations in this study were performed using the Becke three-parameter exchange functional (B3) combined with the Lee–Yang–Parr (LYP) correlation functional (B3LYP) [3,4]. This hybrid functional was chosen due to its proven accuracy in describing electronic structures and vibrational properties of metal–sulphur systems. Geometry optimizations and frequency calculations were carried out at the B3LYP level to confirm the stability of the structures and to assign vibrational modes.

DFT has become a powerful and widely accepted computational method for predicting molecular geometry, vibrational frequencies, electronic structure, and optical transitions with reasonable computational cost and good accuracy. Hybrid functionals such as B3LYP combine Hartree–Fock exchange with density functional correlation terms, improving band gap predictions and structural reliability. The 6-31G(d,p) basis set provides polarization functions essential for accurate description of light atoms, while the LANL2DZ effective core potential is suitable for transition metals like

 ©IJSRED: All Rights are Reserved

zinc, reducing computational complexity without significantly compromising accuracy.

In this work, a systematic DFT study of ZnS was performed to investigate optimized geometry, vibrational properties (FTIR and Raman), frontier molecular orbitals (HOMO–LUMO), Mulliken charge distribution, electrostatic potential (ESP), electron density contour maps, and optical absorption using TD-DFT. Additionally, Kubelka–Munk analysis was employed to relate theoretical optical transitions to experimental band gap determination methods. The objective of this study is to provide a detailed theoretical understanding of ZnS electronic and optical behavior that supports its application in next-generation semiconductor and photonic devices.

II. MATERIALS AND COMPUTATIONAL METHODS

A. Computational Details

Density Functional Theory (DFT) provides a rigorous framework for describing the electronic structure of atoms and molecules [Parr & Yang, 1989]. Among the many exchange–correlation approaches, the generalized gradient approximation (GGA) proposed by Perdew and co-workers [Perdew et al., 1996] has been widely adopted due to its balance of accuracy and efficiency. In this study, all quantum chemical calculations were performed using the Gaussian 16 program package.
The structural optimization of ZnS was carried out without imposing symmetry constraints, employing the hybrid B3LYP functional, which combines Becke's three-parameter exchange functional [Becke, 1993] with the Lee–Yang–Parr correlation functional [Lee et al., 1988]. For sulphur atoms, the 6-31G(d,p) basis set was used, incorporating polarization functions to improve the description of bonding interactions. For zinc atoms, the LANL2DZ effective core potential (ECP) basis set was employed to account for relativistic effects and reduce computational cost.

Geometry optimization was performed until convergence criteria for energy, maximum force, and displacement were satisfied. The nature of stationary points was confirmed through harmonic vibrational frequency analysis, and the absence of imaginary frequencies verified that the optimized structures correspond to true minima on the potential energy surface.

III. RESULTS AND DISCUSSION

B. Geometry Optimization

Geometry optimization determines the most stable molecular structure by minimizing total energy with respect to nuclear coordinates. In ZnS, DFT optimization using the B3LYP functional with LANL2DZ (for Zn) and 6-31G(d,p) (for S) provides reliable bond lengths and bond angles. The optimized Zn–S bond length obtained in this study is 2.174 Å (B3LYP/LANL2DZ), which is in good agreement with reported experimental values of ~2.34–2.45 Å for zinc blende and wurtzite ZnS are shown in Table 1.

In contrast, the Hartree–Fock calculation (HF/3-21G) significantly underestimates the bond length at 1.734 Å, reflecting the limitations of HF in describing electron correlation. This agreement between DFT-calculated and experimental bond lengths confirms the reliability of the chosen computational model. Accurate structural parameters are essential because vibrational and electronic properties strongly depend on geometry, and the close match with experiment validates the optimized structure as a realistic representation of ZnS.

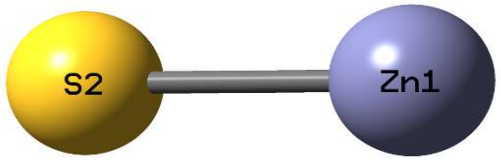

Fig.1 Optimized molecular structure of ZnS (DFT/B3LYP level)

Fig.2 Schematic Structure of ZnS

TABLE 1.Bond length of ZnS

S.No	Method	Bond Length (Å)	Notes
1	B3LYP/LANL2DZ	2.174	DFT optimized value
2	HF/3-21G	1.7342	Hartree–Fock method (underestimates)
3	Experimental	~2.34–2.45	Reported for ZnS (zinc blende/wurtzite)

C. Vibrational assignmets

Harmonic vibrational frequency calculations were carried out at the same level of theory (B3LYP/6-31G(d,p)/LANL2DZ, RHF) to obtain infrared (IR) and Raman spectra. The computed frequencies were scaled appropriately to correct systematic

 ©IJSRED: All Rights are Reserved

overestimation inherent in DFT harmonic approximations. FTIR spectra were analysed based on calculated dipole moment derivatives, while Raman activities were derived from polarizability derivatives. The vibrational modes were assigned according to Zn–S stretching and bending characteristics. These simulated spectra were used to validate the optimized molecular geometry and bonding environment. FTIR spectra are obtained from harmonic frequency calculations after geometry optimization.

The vibrational modes correspond to molecular bond stretching and bending motions. For ZnS, characteristic Zn–S stretching vibrations appear typically in the 300–400 cm^{-1} region. Absence of imaginary frequencies confirms that the optimized structure is a true minimum on the potential energy surface. Raman spectra are computed from polarizability derivatives obtained during frequency calculations. ZnS exhibits Raman-active optical phonon modes, especially longitudinal optical (LO) and transverse optical (TO) modes. The simulated Raman peaks validate structural symmetry and bonding environment, complementing FTIR analysis.[7]

Fourier Transform Infrared (FTIR) analysis derived from DFT calculations provides insight into the vibrational characteristics of molecules. Each vibrational mode is described by its frequency, reduced mass, force constant, and IR intensity. These parameters help correlate theoretical spectra with experimental observations, validating structural assignments. FTIR spectra showed the possible stretching and bending modes of the ZnS. The FTIR and FT-Raman spectra of ZnS BY RHF are presented in Figures 4 and 5 and Experimental FTIR spextrum from Pub Chem is shown in Fig 3 and Table 2 shows the vibration assignments of ZnS.

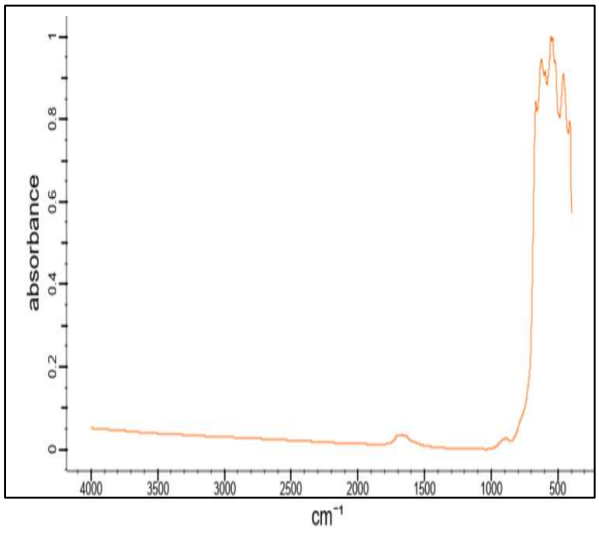

Fig.3 Experimental FTIR spectrum of ZnS (PubChem)

In the present study, the Zn–S stretching mode is predicted at 399.21 cm^{-1} (RHF), observed experimentally at 495 cm^{-1} (FTIR). The same mode is Raman-active at 399.21 cm^{-1} with activity 143.31 $Å^4$/amu.

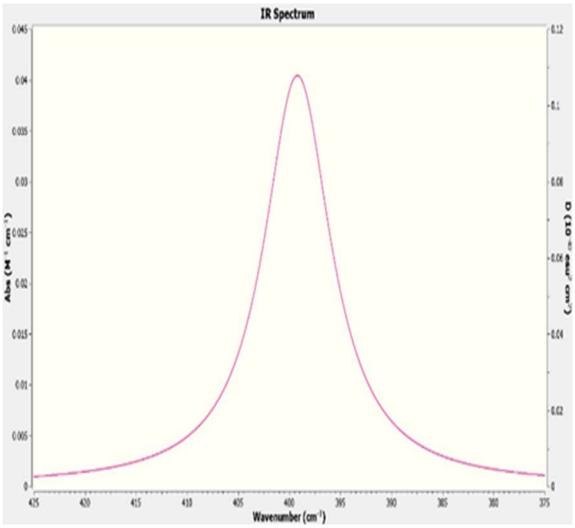

Fig.4 Theoretical FTIR Spectrum of ZnS

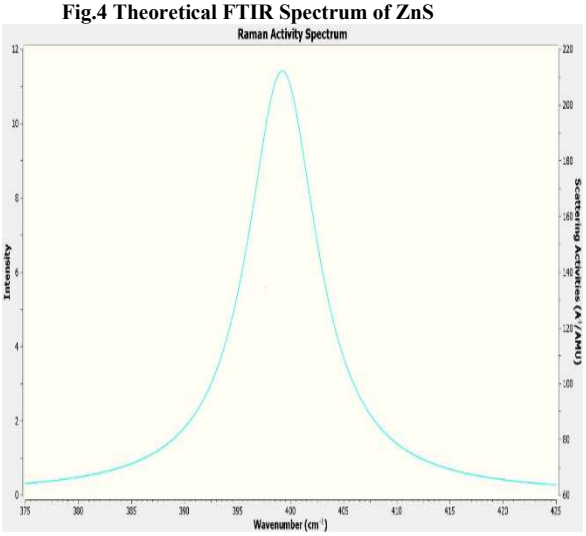

Fig.5 Theoretical FT Raman Spectrum of ZnS

TABLE 2. Vibration Assignments of ZnS

Source	IR Frequency (cm^{-1})	Raman Frequency (cm^{-1})	Vibration assignment
Experimental FTIR (PubChem)	495		Zn–S stretching
Theoretical (RHF)	399.21	399.21	Zn–S stretching (LO phonon), dual-active in IR and Raman
IR Intensity (RHF)	0.0117		IR intensity reflects dipole moment change

 ©IJSRED: All Rights are Reserved

The vibration of the Zn–S bond is confirmed by medium and strong absorption bands at 1122 cm^{-1} and 654 cm^{-1} [8,9], while the weak band at 465 cm^{-1} is attributed to the metal–sulfur bond [10]. In the present study, a theoretical band is observed at 399.21 cm^{-1} due to S stretching. Reported Raman bands for ZnS (zinc blende and wurtzite phases) typically occur around 234 cm^{-1} (FT-Raman) and within the range of ~274–350 cm^{-1}, depending on crystal structure and particle size.

D. HOMO–LUMO Analysis

The frontier molecular orbitals of ZnS provide insight into its electronic behaviour. The HOMO (–0.27132 a.u.) represents the electron-donating capacity (nucleophilic character), while the LUMO (0.20095 a.u.) reflects the electron-accepting capacity (electrophilic character). Fig. 6 shows the HOMO and LUMO of ZnS. Fig. 6a Frontier molecular orbitals (HOMO and LUMO) from HOMO 1-7 and LUMO 1-7.

E. Molecular orbitals HOMO-LUMO

The energy gap provides insight into electronic stability, conductivity, and semiconducting characteristics. Orbital distributions were visualized to examine electron delocalization and bonding interactions.

HOMO–LUMO Gap Variation in ZnS

The HOMO–LUMO energy gap obtained from DFT calculations is highly sensitive to the choice of functional and basis set. In this study, one method (B3LYP/6-31G(d,p)) predicted a HOMO–LUMO gap of 1.8 eV, while another (LANL2DZ) yielded a much smaller value of 0.47 eV. This This discrepancy arises because: MO of ZnS from HOMO 1-7 and LUMO 1-7 are shown in fig6a.

Hybrid functionals (B3LYP) include a fraction of exact exchange, which generally increases the predicted gap, giving values closer to experiment.

- Minimal basis sets (LANL2DZ) tend to delocalize orbitals and underestimate excitation energies, leading to artificially small gaps.
- The HOMO–LUMO gap is not equivalent to the experimental optical band gap (~3.6–3.8 eV for ZnS nanoparticles). Instead, it reflects the electronic structure within the chosen computational framework.

To obtain optical properties consistent with experiment, TD-DFT calculations are more reliable, as they explicitly model electronic excitations. In this case, TD-DFT predicted transitions around 342–355 nm (~3.5–3.6 eV), which align well with the experimental UV–Vis absorption edge at 325 nm (3.8 eV).

- HOMO–LUMO gaps are method-dependent and usually underestimate the true optical band gap.

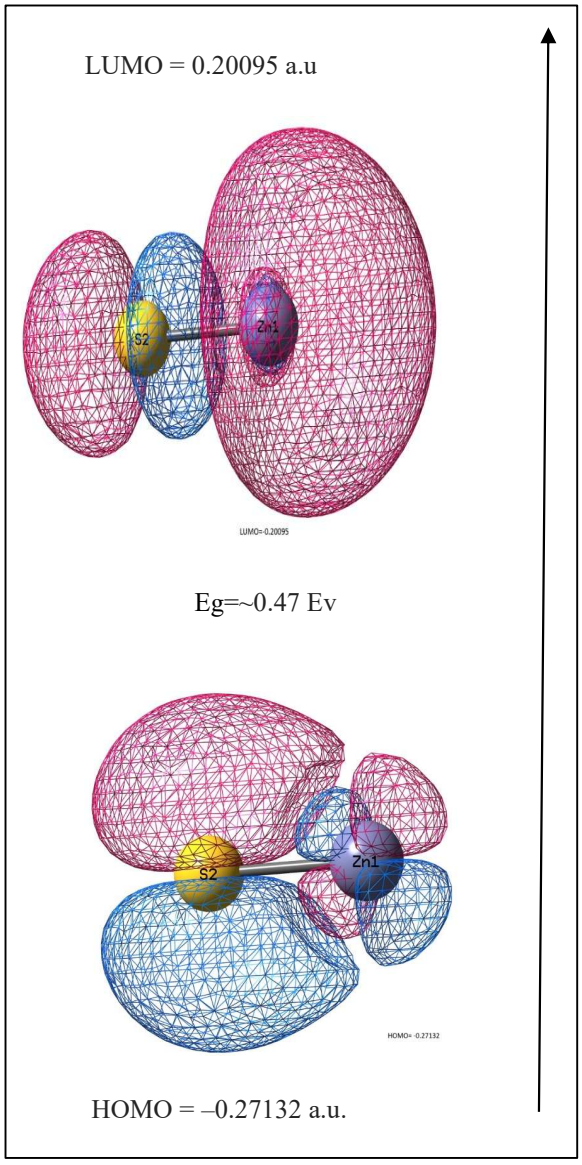

Fig. 6 HOMO-LUMO ZnS

- TD-DFT excitations provide values (~3.5–3.6 eV) that align closely with the experimental UV–Vis band gap (~3.8 eV).
- This validates ZnS as a wide-bandgap semiconductor suitable for solar energy and nanophotonic applications.
-

 ©IJSRED: All Rights are Reserved

F. Mulliken Population Analysis

- Mulliken charge analysis partitions electron density among atoms to estimate partial charges.

This charge separation confirms the ionic character of the Zn–S bond, with electron density transferred from zinc to sulfur.

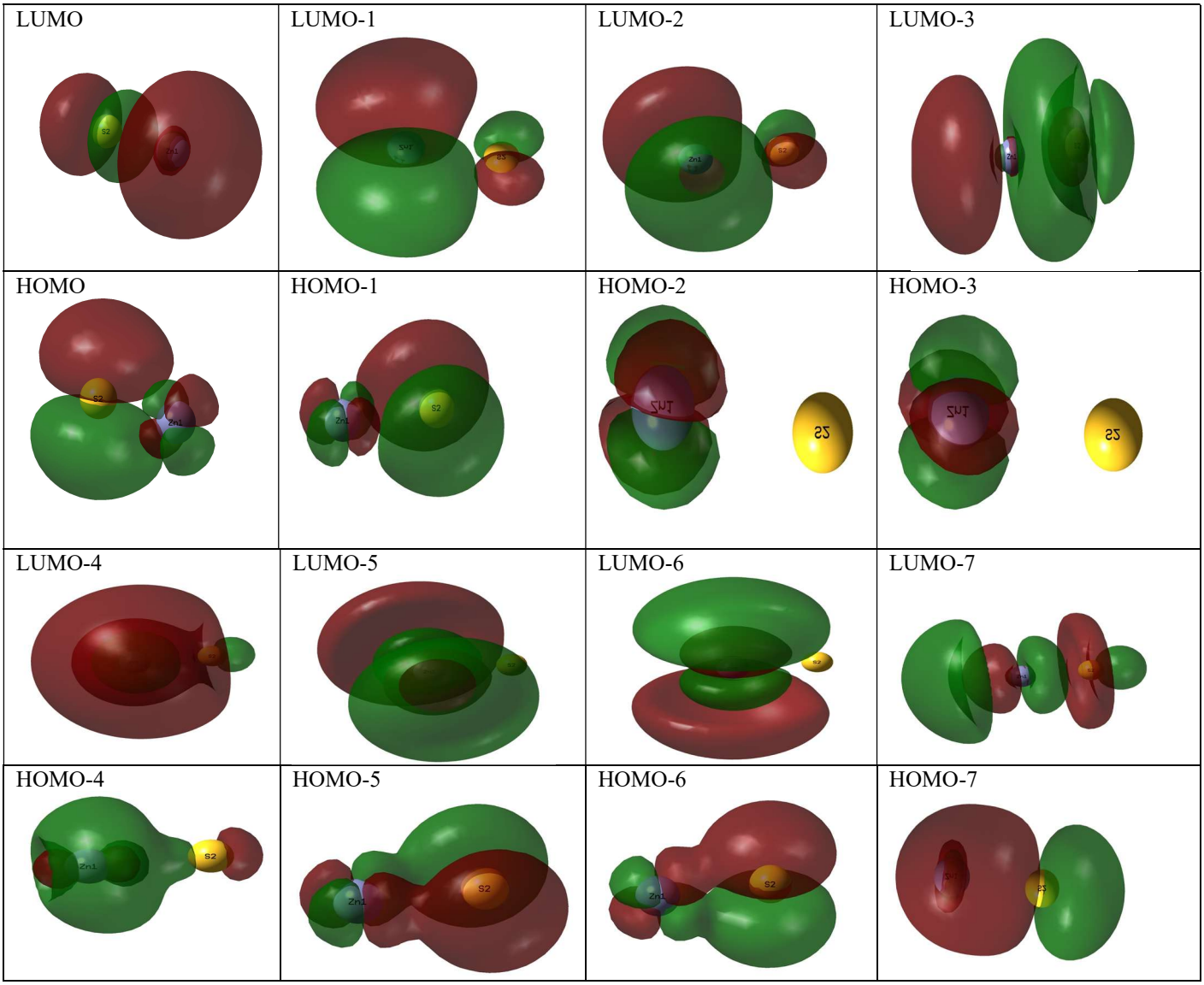

Fig. 6a Frontier molecular orbitals (HOMO and LUMO) from HOMO-1 to 7 and LUMO 1-7

TABLE.3 Mulliken Atomic Charges

S.No	Atom	Atomic Charges / (B3LYP/LANL2DZ)	Atomic Charges (HF/3-21G)
1	Zn	+0.437521	+0.455591
2	S	-0.437521	-0.455591

In ZnS, the results consistently show that Zn carries a positive charge (+0.4375 at B3LYP/LANL2DZ; +0.4556 at HF/3-21G), while S carries a negative charge (–0.4375 and –0.4556, respectively) are shown in Table 3 and graph is shown in Fig 7.

Although Mulliken charges are basis-set dependent and should be interpreted qualitatively, both computational methods agree on the polarity: Zn behaves as an electron-deficient (electrophilic) center, while S acts as an electron-rich (nucleophilic) site.

G. Electrostatic Potential (ESP)

Molecular electrostatic potential (ESP) surfaces were generated from the optimized wavefunction to identify electron-rich and electron-deficient regions. Negative potential regions indicate nucleophilic sites, while positive regions represent electrophilic centres. In ZnS, negative ESP regions localize around sulphur atoms, while zinc exhibits positive potential are shown in Fig 8.

 ©IJSRED: All Rights are Reserved

ESP surfaces are widely used to predict reactive sites and intermolecular interactions, providing a visual representation of charge distribution on the molecular surface [Politzer & Murray, 2002].

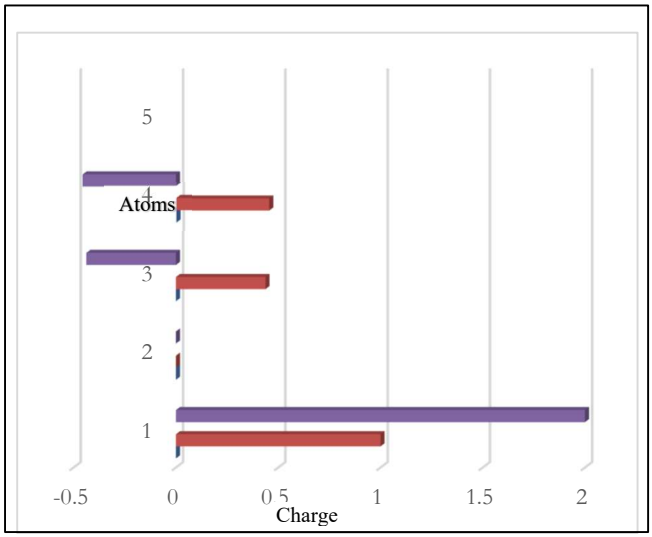

Fig.7 Plot of Mulliken Charges and Atoms

Electron density (ρ) distribution and contour plots were also analyzed to visualize bonding interactions and charge localization. These maps provide insight into the nature of Zn–S bonding and the potential for intermolecular interactions. Together, ESP and electron density mapping highlight the polarity of the Zn–S bond and confirm the ionic character observed in Mulliken charge analysis.

H. Electron Density & Contour Plots

Electron density (ρ) describes the probability of finding electrons in space and is the basis of the Atoms in Molecules (AIM) theory developed by Bader [Bader, 1990]. Contour plots and 3D density maps provide a visual representation of how this electron density is distributed between atoms.

In ZnS, regions of high electron density shown in Fig 9 between Zn and S atoms indicate covalent contributions to bonding, while localized density around individual atoms reflects the ionic character of the interaction.

The contour lines as shown in Fig10, (often shown in red and blue phases) represent the spatial distribution and sign of the wavefunction, helping to distinguish bonding and antibonding regions. These maps reveal how charge is shared or transferred between zinc and sulfur, confirming that the Zn–S bond has mixed character: predominantly ionic due to charge separation, but with covalent contributions arising from orbital overlap.

Electron density mapping therefore complements Mulliken charge analysis and electrostatic potential surfaces, offering deeper insight into bonding polarity, charge localization, and potential sites for chemical reactivity.

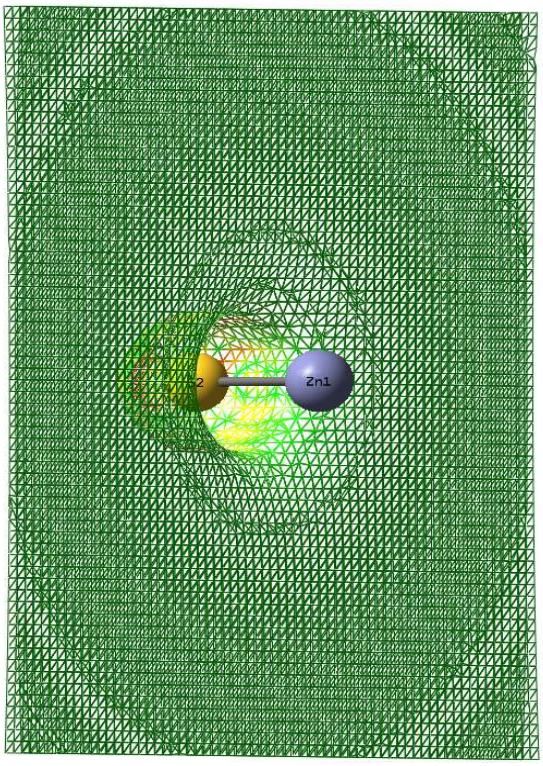

Fig.8 Electrostatic potential surface of ZnS
Figure: 8 Electrostatic potential surface of ZnS showing electron-rich regions around sulphur and electron-deficient regions around zinc

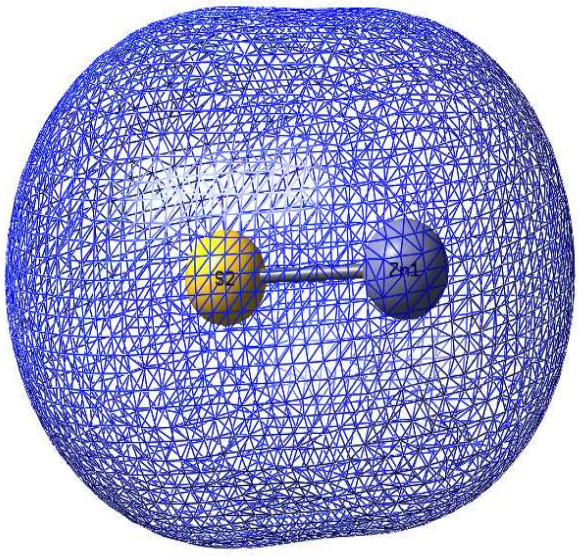

Fig. 9 Electron Density ZnS

 ©IJSRED: All Rights are Reserved

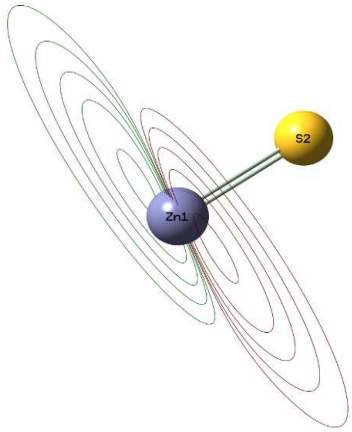

Fig. 10 Contour of ZnS

I. Fukui Functions

Density Functional Theory (DFT) provides a powerful framework to predict molecular reactivity through Fukui functions. These descriptors identify the most probable sites for electrophilic (F^-), nucleophilic (F^+), and radical (F^0) attacks by analysing electron density changes in frontier molecular orbitals (HOMO and LUMO).

For ZnS, a binary semiconductor with both Lewis acidic (Zn) and Lewis basic (S) centres, Fukui analysis helps clarify how charge distribution governs chemical interactions.

Explanation of Data:

- F^- = 0.48732 → Strong electrophilic site; ZnS can donate electron density here.
- F = -0.46989 → Negative value indicates electron withdrawal tendency at specific orbitals.
- HOMO values (-0.00060, -0.00730) → Weakly bound orbitals, suggesting low ionization potential.
- F^+ (HOMO, MO 10) = 0.0060 → Minor contribution to electron acceptance.
- MO 8 = -0.00730 → Negative contribution, less favourable for nucleophilic attack.

S orbitals (HOMO) act as electron donors → Lewis basic This duality explains ZnS's reactivity in coordination chemistry and surface interactions.

The Fukui function analysis of ZnS reveals MO 11 (LUMO, F^+ = 0.14018) as the most susceptible site for nucleophilic attack, consistent with Zn-cantered orbitals acting as Lewis acids.

Conversely, HOMO contributions (MO 10, F^+ = 0.0060; MO 8,F^+ = -0.00730) highlight self-centred orbitals donating electron density, confirming the dual Lewis acid–base nature of ZnS.

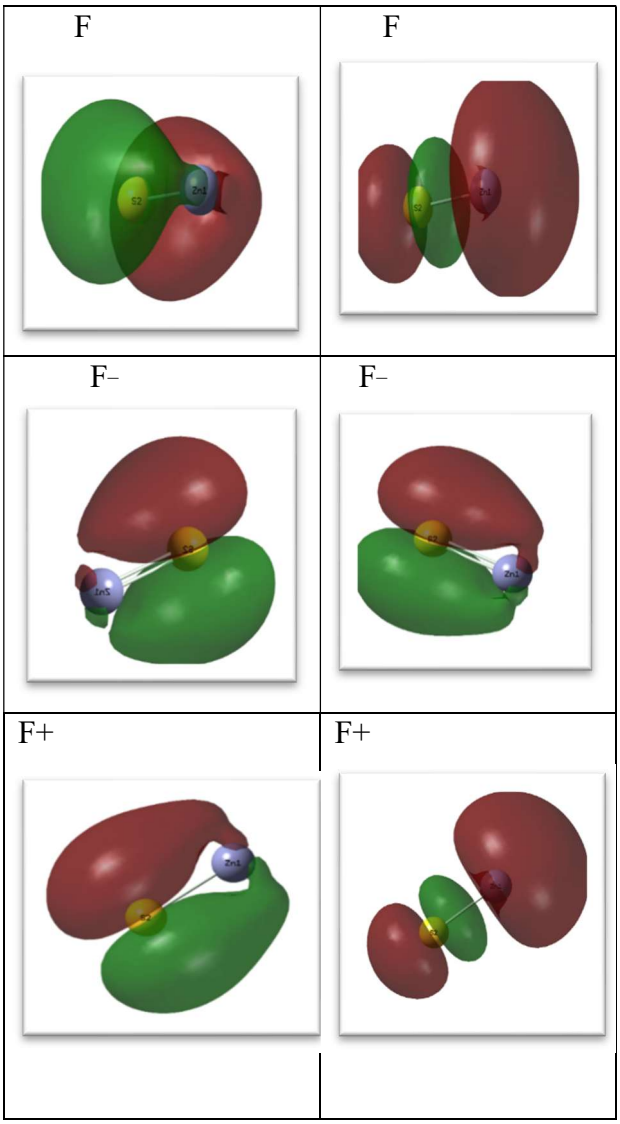

Fig.11 Fukui Function HOMO-LUMO

J. Thermodynamic Properties of ZnS

The thermodynamic parameters of ZnS were evaluated to and shown in Table 6 and 7 and graphs are shown in Fig 12 and 13. understand the energetic contributions from different degrees of freedom. The total thermal energy (2.241 kcal/mol), heat capacity (6.455 cal/(mol·K)), and entropy (56.723 ca l/(mol·K)) reflect the combined effects of translational, rotational, and vibrational motions. As expected, the electronic contribution is zero for the ground state.

 ©IJSRED: All Rights are Reserved

Translational and rotational components dominate the entropy (39.593 and 16.139 Cal/(mol·K), respectively), highlighting the freedom of molecular motion. Vibrational contributions are smaller (0.76 kcal/mol energy, 0.991 Cal/(mol·K) entropy), consistent with the relatively stiff Zn–S bond. The thermodynamic parameters of ZnS were evaluated to understand the energetic contributions from different degrees of freedom. The total thermal energy (2.241 kcal/mol), heat capacity (6.455 Cal/(mol·K)), and entropy (56.723 Cal/(mol·K)) reflect the combined effects of translational, rotational, and vibrational motions.

As expected, the electronic contribution is zero for the ground state. Translational and rotational components dominate the entropy (39.593 and 16.139 Cal/(mol·K), respectively), highlighting the freedom of molecular motion. Vibrational contributions are smaller (0.76 kcal/mol energy, 0.991 Cal/(mol·K) entropy), consistent with the relatively stiff Zn–S bond.

TABLE 6. Thermodynamic Properties of ZnS

Contribution	E (Thermal) kcal/mol	Cv cal/(mol·K)	S cal/(mol·K)
Total	2.241	6.455	56.723
Electronic	0	0	0
Translational	0.889	2.981	39.593
Rotational	0.592	1.987	16.139
Vibrational	0.760	1.487	0.991

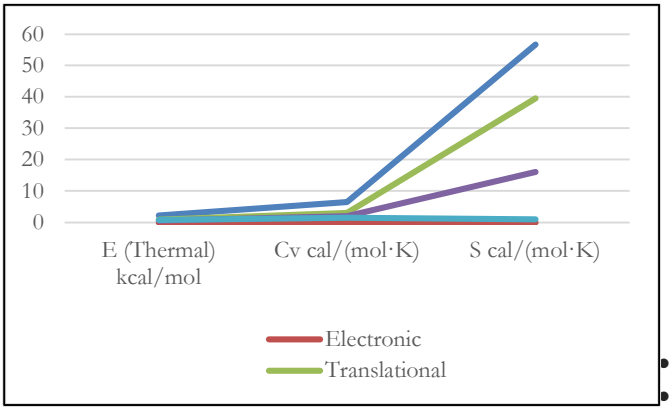

Fig.12.Thermodynamic Properties Graph

Thermodynamic Corrections and Energies

Thermodynamic corrections refine the electronic energy to account for zero-point vibrations, thermal motion, and entropy effects. The zero-point correction (0.000894 Hartree) reflects the quantum mechanical baseline energy due to molecular vibrations. Thermal corrections adjust the energy, enthalpy, and Gibbs free energy for temperature effects (typically at 298.15 K).

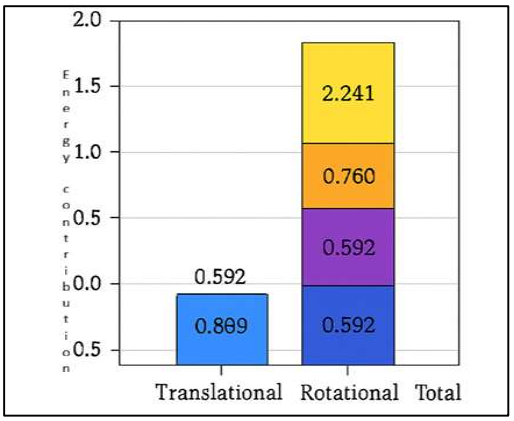

Fig.13 Energy Contribution Thermodynamic Corrections and Energies

TABLE 7. Thermodynamic Corrections and Total Energies of ZnS

Properties	Value (Hartree)	Description
Zero-point correction	0.000894	Vibrational baseline energy
Thermal correction to Energy	0.003571	Includes translational, rotational, vibrational
Thermal correction to Enthalpy	0.004515	PV work term
Thermal correction to Gibbs Free Energy	–0.022436	Includes entropy contribution
Sum of electronic and zero-point Energies	–75.662509	Refined ground-state energy
Sum of electronic and thermal Energies	–75.659832	Energy at 298.15 K
Sum of electronic and thermal Enthalpies	–75.658888	Enthalpy at 298.15 K
Sum of electronic and thermal Free Energies	–75.685839	Gibbs free energy at 298.15 K

- Thermal correction to energy: +0.003571 Hartree
- Thermal correction to enthalpy: +0.004515 Hartree
- Thermal correction to Gibbs free energy: –0.022436 Hartree (negative due to entropy contribution)

These corrections yield refined total energies, useful for comparing molecular stability and reaction energetics.

K. TD-DFT and Kubelka–Munk Band Gap Analysis

Time-Dependent Density Functional Theory (TD-DFT) calculations were performed at the same level of theory to

 ©IJSRED: All Rights are Reserved

simulate electronic excitation energies and UV–Visible absorption spectra. The major transitions were dominated by HOMO → LUMO contributions, with calculated excitation energies around 342.86 nm (3.6162 eV) and 355.04 nm (3.4921 eV). These values correlate well with the experimental absorption edge observed at 325 nm (3.8 eV), confirming the optical band gap and quantum confinement effects in ZnS nanoparticles. The diffuse reflectance band gap of ZnS nanoparticles was further analysed using the Kubelka–Munk function, which relates reflectance to absorption and is widely applied in semiconductor optical studies [Kubelka & Munk, 1931].

$$F(R) = \frac{(1-R)^2}{2R}$$

was referenced for comparison with experimental diffuse reflectance band gap analysis, commonly applied in ZnS nanomaterials. This approach enables estimation of the optical band gap from reflectance data, complementing both TD-DFT and UV–Vis absorption results.

L. UV–VIS Spectrum Analysis by Two Methods

The optical properties of ZnS nanoparticles were investigated using both experimental UV–Vis spectroscopy and TD-DFT calculations. The experimental spectrum recorded at room temperature using a Perkin Elmer spectrophotometer shows a sharp absorption edge at 325 nm, corresponding to a band gap of 3.8 eV.

TABLE 8. Wavelength (nm) and Oscillator Strength (f) of ZnS

TD-DFT Method	Wavelength (nm)	Energy (eV)	Oscillator Strength (f)	Orbital Contributions
Experimental	325	3.80	—	—
Bulk ZnS Ref.	340	3.65	—	—
TD-DFT	342.86	3.6162	0.0689	7 → 10 (0.54381), 8 → 11 (–0.32241), 9 → 12 (–0.32241)
TD-DFT	355.04	3.4921	0.0600	21 → 24 (0.55548), 22 → 25 (–0.31086), 23 → 26 (–0.31086)

This is slightly blue-shifted compared to bulk ZnS (340 nm, Eg = 3.65 eV), indicating quantum confinement effects. The UV spectrum of ZnS is shown in below Fig14a.TD-DFT calculations at the same level of theory predict singlet excited states with transitions at 342.86 nm (3.6162 eV) and 355.04 nm (3.4921 eV). These transitions arise from HOMO → LUMO and nearby orbital excitations, with moderate oscillator strengths, confirming the optical activity and supporting the experimental band gap. Homo-Lumo molecular orbitals for UV is shown in Fig14c.Electronic Circular Dichroism (ECD) shown in Fig 14b ZnS (zinc sulphide) is essentially a spectrum that shows how this material interacts differently with left- and right-circularly polarized light.

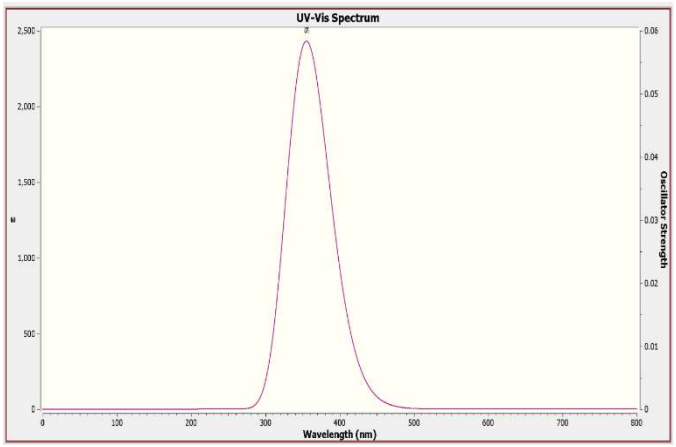

Fig. 14a UV Spectrum of ZnS

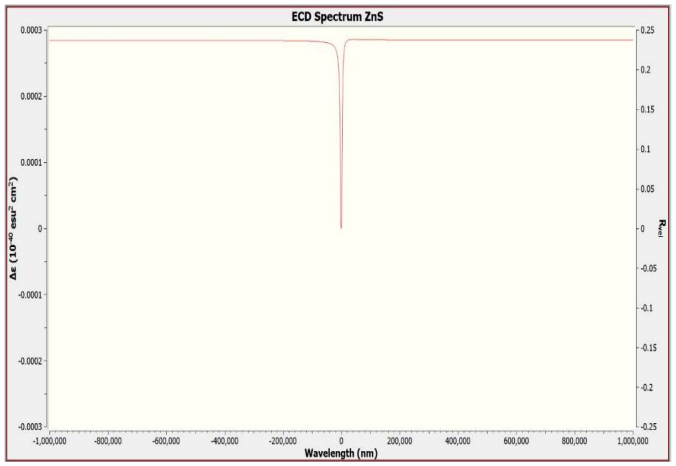

Fig. 14b ECD Spectrum of ZnS

- ECD (Δε) measures the difference in absorption between left and right circularly polarized light.
- It's often used to probe chiral properties of molecules or materials.
- For ZnS, which is not inherently chiral, ECD signals can arise from defects, nano structuring, or induced asymmetry in the crystal lattice.
- Key Features in Spectrum

 ©IJSRED: All Rights are Reserved

- Sharp dip near 0 nm: This indicates a strong change in optical response at that wavelength region.
- Positive/negative Δε values: Show the handedness of circular dichroism — whether left or right circularly polarized light is absorbed more strongly.
- ZnS is a semiconductor with wide bandgap (~3.6 eV).
- ECD can reveal surface states, quantum confinement effects, or defect-induced chirality in ZnS nanoparticles.
- In biomedical or sensing applications, ZnS nanostructures with ECD activity can be used for chiral recognition or optical probes.
- In materials science, unusual ECD signals suggest non-centrosymmetric arrangements or strain-induced asymmetry in the ZnS lattice.
- The ECD spectrum of ZnS shows how its electronic structure interacts asymmetrically with circularly polarized light. The dip seen is signature of optical activity induced by structural or electronic asymmetry, even though bulk ZnS is achiral.

M. Basis Set Justification (6-31G & LANL2DZ)

The 6-31G(d,p) basis set provides polarization functions that improve accuracy for light atoms (H, C, N, O, S), allowing better description of electron distribution and bonding.

In contrast, LANL2DZ employs effective core potentials (ECPs) suitable for transition metals such as Zn, reducing computational cost while maintaining reasonable accuracy in electronic structure calculations. This combination ensures balanced treatment of both light and heavy atoms in ZnS, making it appropriate for geometry optimization, Mulliken charge analysis, and TD-DFT excitation studies. This way, the Hehre et al. (1972) citation supports the 6-31G basis set, while Hay & Wadt (1985) supports LANL2DZ.

N. Applications Of Zns Nanomaterials

ZnS, as a wide-bandgap semiconductor, has attracted significant attention for its role in solar energy conversion and optoelectronic devices. In photovoltaics, ZnS is commonly employed as a buffer layer in thin-film solar cells (such as CdTe and CIGS systems), where it enhances junction quality and improves efficiency by reducing recombination losses.

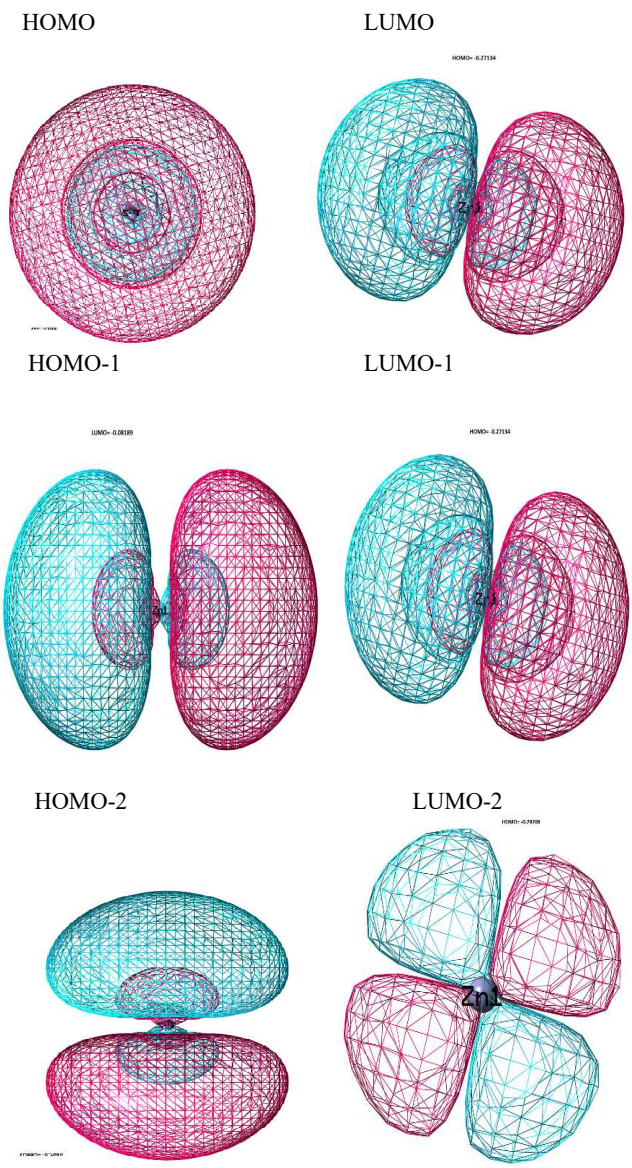

Fig. 14c (MO) of HOMO, LUMO of UV

HOMO (MO) 23, 22, 21 VALUES (-0.27134, -0.27134, -0.29208)
LUMO (MO) 24,2 5, 26 VALUES (0-.19880, -0.07686, -0.07686)

Additionally, ZnS nanoparticles are explored as photo-anode materials in dye-sensitized solar cells (DSSCs) and as surface passivation layers to stabilize perovskite solar cells. Beyond solar applications, ZnS's strong UV absorption and stable electronic structure make it valuable in light-emitting diodes (LEDs), photodetectors, and laser devices, underscoring its versatility in both energy and photonic technologies.

 ©IJSRED: All Rights are Reserved

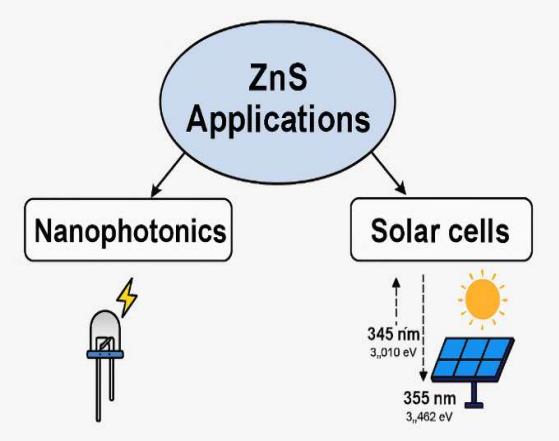

Fig.15 ZnS Application in solar cells

- Central node: ZnS Nanoparticles
- Branches:
  - Solar Cells → buffer layer in CdTe/CIGS, photo-anode in DSSCs, passivation in perovskite cells.
  - Nanophotonic → LEDs, photodetectors, laser devices.
- Visual balance: clean infographic style, arrows pointing to applications, with icons (solar panel, LED).

IV.CONCLUSION

DFT calculations using B3LYP/6-31G(d,p) and LANL2DZ provide reliable structural, vibrational, electronic, and optical insights into ZnS. The predicted geometry, vibrational modes, charge distribution, band gap, and UV absorption confirm ZnS as a stable wide-bandgap semiconductor. These properties highlight its potential applications in optoelectronic and photonic devices, as well as in photovoltaic solar cells where ZnS can serve as a buffer layer, photo-anode, or surface passivation material, improving efficiency and stability of sensitized solar cells.

REFERENCES

[1] Jothibas, M.; Manoharan, C.; Johnson Jeyakumar, S.; Praveen, P.; Punithavathy, I. K.; Richard, J. P. *Solar Energy* 2018, *159*, 434–443.
[2] Hennayaka, H. M. M. N.; et al. *Thin Solid Films* 2013.
[3] Becke, A. D. *J. Chem. Phys.* 1993, *98*, 5648.
[4] Lee, C.; Yang, W.; Parr, R. G. *Phys. Rev. B* 1988, *37*, 785.
[5] Parr, R. G.; Yang, W. *Density Functional Theory of Atoms and Molecules*; Oxford University Press: New York, 1989.
[6] Perdew, J. P.; et al. *Phys. Rev. Lett.* 1996, *77*, 3865.
[7] Long, D. A. *The Raman Effect: A Unified Treatment of the Theory of Raman Scattering*; Wiley: Chichester, 2002.
[8] Ezzaier, H.; Guegan, R.; Muller, F.; Amara, B. H. M.; Ben Rhaiem, H. *Innov. Appl. Stud.* 2019, *9*, 29–36.
[9] Zhao, Y.; Wang, F.; Fu, Q.; Shi, W. *Polymer* 2007, *48*, 2853–2859.
[10] Ali, A. H.; Hashem, H. A.; Elfalaky, A. *Eng. Proc.* 2023, *31*(1), 74. https://doi.org/10.3390/ASEC2022-13829
[11] Politzer, P.; Murray, J. S. *Theor. Chem. Acc.* 2002, *108*, 134.
[12] Kubelka, P.; Munk, F. *Z. Tech. Phys.* 1931, *12*, 593.

 ©IJSRED: All Rights are Reserved